IJMGE

Int. J. Min. & Geo-Eng.
Vol.48, No.2, December 2014, pp.115-126.

A Novel Integrated Approach to Modelling of Depletion-Induced Change in Full Permeability Tensor of Naturally Fractured Reservoirs

Zahra Izadi, Mohammad Ali Aghighi*

Imam Khomeini International University, Ghazvin, Iran

Received 5 May 2014; Received in revised form 30 August 2014; Accepted 5 Dec 2014
Corresponding author: m.aghighi@ut.ac.ir

Abstract
More than half of all hydrocarbon reservoirs are Naturally Fractured Reservoirs (NFRs), in which production forecasting is a complicated function of fluid flow in a fracture-matrix system. Modelling of fluid flow in NFRs is challenging due to formation heterogeneity and anisotropy. Stress sensitivity and depletion effect on already-complex reservoir permeability add to the sophistication. Horizontal permeability anisotropy and stress sensitivity are often ignored or inaccurately taken into account when simulating fluid flow in NFRs. The aim of this paper is to present an integrated approach for evaluating the dynamic and true anisotropic nature of permeability in naturally fractured reservoirs. Among other features, this approach considers the effect of reservoir depletion on reservoir permeability tensor, allowing more realistic production forecasts. In this approach the NFR is discretized into grids for which an analytical model yields full permeability tensors. Then, fluid flow is modelled using the finite-element method to obtain pore-pressure distribution within the reservoir. Next, another analytical model evaluates the change in the aperture of individual fractures as a function of effective stress and rock mechanical properties. The permeability tensor of each grid is then updated based on the apertures obtained for the current time step. The integrated model proceeds according to the next prescribed time increments.

Keywords: *depletion effect, fracture aperture, naturally fractured reservoirs, permeability tensor*.

1. Introduction

One of the major factors affecting fluid flow in naturally fractured reservoirs is fracture permeability, which is hard to determine, as NFRs are often heterogeneous and anisotropic. In order to model fluid flow in NFRs, several approaches have been used: single continuum [1-4], multiple continuum [4-8] and discrete fracture [9-12]. A full and effective permeability tensor for each block effectively represents the network of arbitrarily oriented and distributed natural fractures in that block [13]. The diagonal permeability entries of this tensor represent the dependence of flow rate on pressure gradient in the same direction,

whereas the off-diagonal permeability entries of this tensor account for the dependence of flow rate in one direction on pressure gradient in the orthogonal direction. A number of studies have been carried out on fluid-flow simulation of NFRs using the concept of effective permeability tensor [10, 11, 14-21].

Reservoir permeability is often considered as a constant value over a reservoir's life. This assumption, particularly in NFRs, causes significant error in production forecasts. The change in fracture permeability induced by pore-pressure reduction has been studied in the laboratory and in the field [22-25].

In this paper we present a novel integrated approach for modelling fluid flow in a porous medium containing a fracture network. In this approach fluid flow is modelled based on the concept of effective permeability tensor. The model has advantages over many existing models in which the off-diagonal permeability entries are neglected. Furthermore, the change in permeability tensor over the reservoir life is taken into account based on the change in fracture aperture resulting from production-induced change in effective stress and rock mechanical properties.

2. Methods

The integrated scheme introduced in this paper consists of three major models: an analytical permeability tensor model, a numerical fluid-flow model, and an analytical geo-mechanics model. The algorithm of this scheme is shown in Figure 1. The procedure consists of the following steps:

I) A number of data sets are inputted into the model. These data sets include reservoir properties, model geometry, rock mechanical properties and fracture geometry.

II) The reservoir is discretized into blocks of appropriate dimensions.

III) An analytical model is used to calculate a full permeability tensor, which includes both diagonals and off-diagonal entries, for each reservoir block.

IV) The Finite Element Method (FEM) is used to model fluid flow in the reservoir where the contribution of arbitrarily oriented natural fractures in fluid flow is taken into account through effective permeability tensors. This model yields nodal pore pressure at each time step.

V) An analytical model is used to evaluate the change in aperture of each fracture due to the reservoir depletion at the current time step. Required data include in-situ stress tensor, rock mechanical properties, pore pressure and initial aperture.

VI) Once the change in aperture is obtained for each fracture, permeability tensor of each element is evaluated and updated. Nodal pore pressure is then obtained for the next time step using the FEM-based fluid-flow model. This procedure continues for a given set of time increment over the course of production. The foregoing models are discussed in following sections.

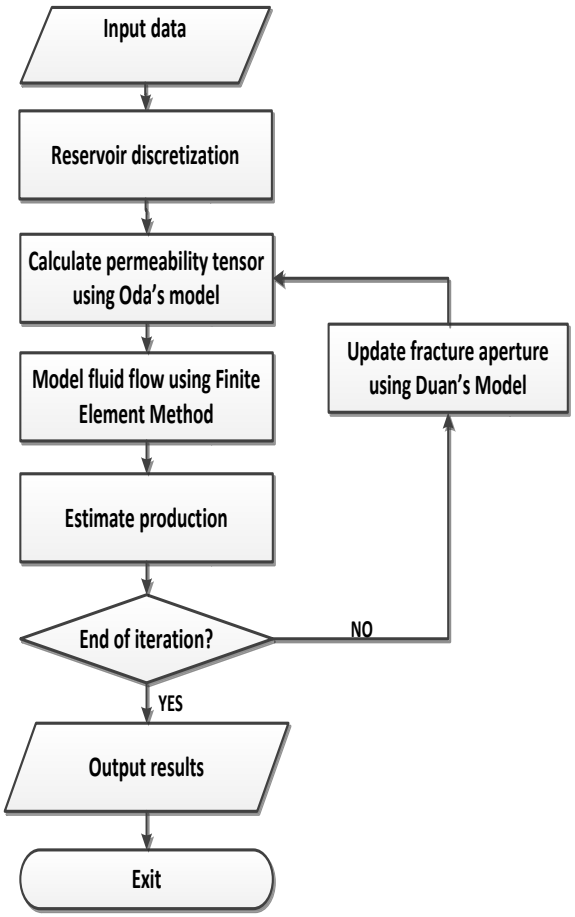

Fig. 1. Algorithm of the integrated model

2.1. Permeability tensor calculation

In this paper the permeability tensor of each reservoir block is calculated using an analytical method presented by Oda [11]. Oda's equation is as follows.

$$k_{ij}^{(f+m)} = \lambda\left(P_{kk}\delta_{ij} - P_{ij}\right) + k^{(m)}\delta_{ij} \quad (1)$$

where k_{ij} is the equivalent permeability tensor, δ_{ij} is the Kronecker delta, $P_{kk}= P_{11}+P_{22}$, the superscript *f* and *m* denote fracture and matrix, respectively, and the subscript *i* and *j* denote tensor indices. As implied by the cubic law, λ is a dimensionless geometric factor approaching $\frac{1}{12}$.

P_{ij} is the 'crack tensor', which is a symmetric second-rank tensor relating only to the geometry of fractures. This tensor can be defined as follows:

$$P_{ij} = \frac{\sum_{k=1}^{N} b_k^3 L_k n_i n_j}{A} \quad (2)$$

where N is the number of fractures, b_k is the aperture of the k^{th} fracture, L_k is the fracture length of the k^{th} fracture, A is the measured area of the plan-view rock face, and n_i and n_j are unit normal vectors. The following assumptions are made for Oda's method.

- Fractures are assumed to be co-planar.
- No fluid head loss at fracture intersections takes place.
- Fractures extend the full thickness of the reservoir bed.
- Fractures are co-planar, i.e., aperture is constant along an individual fracture.
- Fractures are interconnected.

As can be seen from Equation 1, Oda's method yields full tensor permeability including both diagonal and off-diagonal entries. This is particularly advantageous when dealing with heterogeneous formations such as NFRs. An off-diagonal entry of the permeability tensor takes account of fluid flow along a certain direction where pressure gradient is along the orthogonal direction. For instance, k_{xy} represents the fluid flow along the y-direction where pressure gradient is along the x-direction. To this effect, the role of arbitrarily oriented fractures in flow is taken into account more realistically.

2.2. Fluid-flow modelling

The general form of diffusivity equation for an incompressible single-phase fluid is as follows:

$$\varnothing c_t \frac{\partial_p}{\partial_t} = \nabla.\left(\frac{k}{\mu}\nabla p\right) \quad (3)$$

where Ø is the effective porosity, c_t is the total system compressibility, p is the pore pressure, t is the time, μ is the fluid viscosity and **k** is the permeability tensor of the formation. The finite-element formulation of Equation 3 is as follows:

$$P=M.f \quad (4)$$

where the pressure vector of the current time step is denoted by **P**, which can be defined as follows:

$$P^T= (p_1 \quad p_2 \quad \dots \quad p_n) \quad (5)$$

where p_1, p_2 and p_n are the pore pressure of the first, second and nth nodes, respectively, at the current time step.

M is the mass matrix, defined as follows:

$$M= L + \Delta t H \quad (6)$$

where **L** and **H** are defined as follows:

$$L = \sum_{e=1}^{ne} L^e \quad (7)$$

$$H = \sum_{e=1}^{ne} H^e \quad (8)$$

in which *ne* is the number of elements and $\mathbf{L}^e$ and $\mathbf{H}^e$ are expanded as follows:

$$L^e = \int_{\Omega^e}\left[\left(c_t^e\right)^{i-1}\left(\varnothing_t^e\right)^{i-1}\left(N_p^e\right)^T N_p^e\right]d\Omega \quad (9)$$

$$H^e = \int_{\Omega^e}\frac{\left(K^e\right)^{i-1}}{\left(\mu^e\right)^{i-1}}\left[\left(\nabla N_p^e\right)^T \nabla N_p^e\right]d\Omega \quad (10)$$

where:

$$N_p^e = \left(N_1 \quad N_2 \quad \dots \quad N_n\right) \quad (11)$$

in which N_1, N_2 and N_n are the shape functions of the first, second and n^{th} elements.

$\left(c_t^e\right)^{i-1}$, $\left(\varnothing_t^e\right)^{i-1}$, $\left(k^e\right)^{i-1}$ and $\left(\mu^e\right)^{i-1}$ in Equations 9 and 10 are the total system compressibility, the total effective porosity, the

permeability tensor and the fluid viscosity of e^{th} element at the previous time step, respectively. As can be seen from Equations 9 and 10, the formulations allow all foregoing system properties to be updated at each time step. For the focus of this paper, i.e., the effect of temporal and spatial change in permeability tensor on the fluid flow in NFRs, the following assumptions are made:

- Total system compressibility is time- and pressure-independent.
- Primary porosity is constant throughout the formation.
- Oda's model is responsible for taking into account the matrix and fracture deformation between consecutive time steps. Hence the FEM fluid-flow model disregards the rock deformation.
- Fracture porosity is negligible with respect to the matrix porosity [26, 27].
- Fluid viscosity is independent of the pressure range applied here and remains constant throughout the reservoir.
- The production here is assumed to be an isothermal process, which is a common assumption in conventional reservoir simulations. Thus, the effect of the formation temperature on the fluid viscosity can be neglected.

In Equation 4, **f** is the force vector, defined as follows:

$$F = L^{i}.P^{i-1} \tag{12}$$

Equation 4 is solved for pore pressure incrementally such that a quasi-static process holds true. In other words it is assumed that no dramatic changes in time-dependent variables such as pore pressure and permeability tensor take place between two consecutive time steps. This is particularly true when dealing with infinitesimal deformation of apertures resulting from depletion.

2.3. Geomechanical model

Pore-pressure reduction during production results in the deformation of the rock system, including matrix and fractures. Contribution of fractures in fluid flow is substantially higher than that of the matrix. Fracture closure induced by pore-pressure depletion results in change in fracture aperture. Shear deformation of fractures usually takes place during reservoir pressurization, which is not the case here. Other types of rock deformation such as block movement and rotation are uncommon during the production process in reservoirs, and are hence neglected here.

Equation 13 calculates the change in fracture aperture [28] by accounting for rock mechanical properties of the matrix, i.e., Poisson's ratio and Young's modulus:

$$\delta = \sqrt{\frac{2b_0^2\left(1-\nu^2\right)\sigma_n'}{E\,\xi}} \tag{13}$$

where δ is the change in fracture aperture, b_0 is the initial average aperture, ν is the Poisson's ratio, σ_n' is the normal effective stress (exerted perpendicular to the fracture wall), E is the Young's modulus, and ζ (sigma) is a ratio reflecting surface topography. The latter value is determined through numerical simulation. In this paper ζ is assumed to be 0.01, following the simulation results presented by Duan et al. [28].

Once nodal pore pressure is obtained from modelling fluid flow at each time step, the change in individual fracture aperture can be evaluated using Equation 13. This is done after the corresponding effective stress acting on the respective fracture is determined from far field stresses and the weighted average pore pressure of the nearest nodes to the fracture centre. Knowing the change in aperture of all fractures, the permeability tensor of each block is recalculated to be used in modelling of fluid flow at the next iteration. This procedure is repeated for all time steps.

3.4. Estimating production

The fluid recovery from a single-phase reservoir depends on the reservoir drive(s) and associated pressure reduction. For a compaction drive in a volumetric process, the following equation can be used [29].

$$V_p = V_i\left(e^{c(p_i-\bar{p})}-1\right) \tag{14}$$

where V_p is the volume of the reservoir block at pressure p, V_i is the initial volume of the reservoir block, c is the pore volume compressibility, p_i is the initial reservoir pressure, and $\bar{p}$ is the average reservoir pressure. Knowing the pore pressure at each

node and time step, the volume of produced fluid can be determined. This calculation is done for each element and the resulting volumes are totalled over the entire reservoir to determine the total volume of produced fluid.

3.5. Validation of FEM-based fluid-flow model with permeability tensor

Equation 3 can be expanded for an anisotropic porous medium as follows:

$$k_{xx}\frac{\partial^2 p}{\partial x^2}+2k_{xy}\frac{\partial^2 p}{\partial x\,\partial y}+k_{yy}\frac{\partial^2 p}{\partial y^2}=\varnothing\mu \qquad (15)$$

Papadopulos' solution [30] to Equation 15 for an infinite-acting radial flow is as follows:

$$\sqrt{k_{xx}k_{yy}-k_{xy}^2}\,\frac{h\left(p_i-p_{x,y,t}\right)}{141.2qB\mu}= -\frac{1}{2}Ei\left[\frac{-\varnothing\mu c_t}{0.001056t}\left(\frac{k_{xx}y^2+k_{yy}x^2-2k_{xy}xy}{k_{xx}k_{yy}-k_{xy}^2}\right)\right] \qquad (16)$$

where k_{xx}, k_{xy}, k_{yy} are the components of the permeability tensor in mD, p_i is the initial reservoir pressure in psi, q is the flow rate in STB/day, μ the fluid viscosity in cp, c_t is the total system compressibility in 1/psi, B is the formation volume factor in bbl/STB [1], h is the pay-zone thickness in ft, t is the time in day, **x** and y are the coordinates in a 2-D Cartesian system, and Ei is the exponential integral function. The numerical solution of Equation 3 obtained from the finite-element method is verified against the foregoing analytical solution (i.e., Eq. 16). Data used for this purpose are shown in Table 1 and the results in Figure 2. As can be seen from Figure 2, a very good match is achieved.

Table 1. Data used for verification of numerical fluid-flow model.

Property/Quantity	magnitude	unit
Reservoir data and geometry		
Reservoir area	7.5×10^6	ft^2
Pay zone thickness	100	ft
Initial pressure	4000	psi
Fluid viscosity	1	cp
k_{xx}	5	mD
k_{xy}	3	mD
k_{yy}	1.2	mD
Matrix porosity	0.2	fraction
Formation volume factor	1	
Flow rate	1000	bbl/day
Total system compressibility	6.33×10^{-6}	1/psi

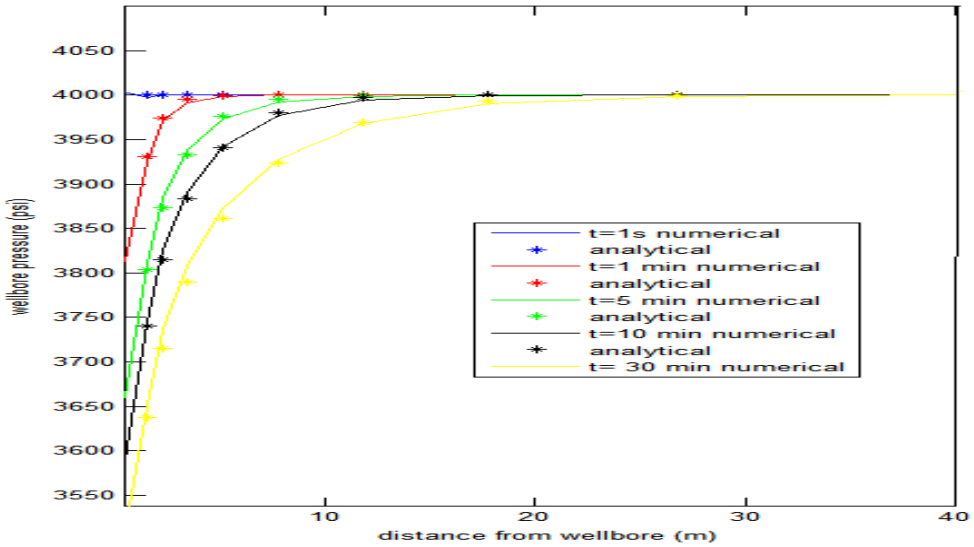

Fig. 2. Verification of fluid-flow model: numerical vs. analytical results

1. Stock Tank Barrel

3. Case study

The integrated approach proposed in this paper is used to investigate the effect of production-induced closure of natural fractures on production forecast. In order to focus on the main idea of the paper only a limited number of fractures are considered. This is despite the fact that real fracture densities are markedly higher than what is considered here. Data used for the case study presented here include model geometry data and fracture characteristics, as well as reservoir fluid and rock mechanical properties. These data are presented in Table 2.

Table 2. Data used for the case study

Property/Quantity	magnitude	Unit
Reservoir data and geometry		
Reservoir area	40000	m^2
well radius	4	in
Pay zone thickness	100	ft
Fluid viscosity	1	cp
Matrix permeability	0.5	mD
Matrix porosity	0.28	dimensionless
Geomechanical properties		
Young's modulus	4.6×10^{6}	psi
Poisson's ratio	0.35	dimensionless
Pore compressibility	6.33×10^{-6}	1/psi
Maximum horizontal stress	7500	psi
Minimum horizontal stress	6500	psi

Fractures are assumed to be vertical, co-planar and well interconnected. Finite-element discretization of the reservoir can be seen in Figure 3. A wellbore is located at the centre of the geometry. The numbers of iso-parametric four-noded elements and nodes are 384 and 392, respectively. Time increments are chosen carefully to comply with the assumption of the production process to be quasi-static. The program is coded in MATLAB®. The reservoir system in this model is a drive mechanism with single-phase flow under isothermal compaction. Figure 4 shows a synthetized fracture network which conforms to the assumptions of Oda's analytical model.

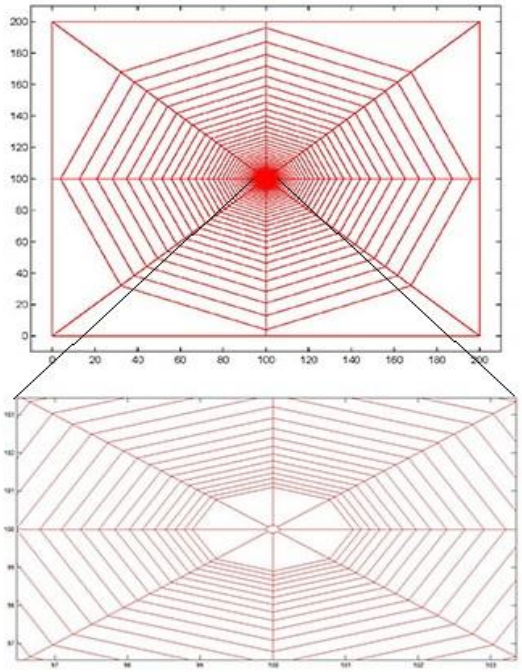

Fig. 3. Finite-element discretization

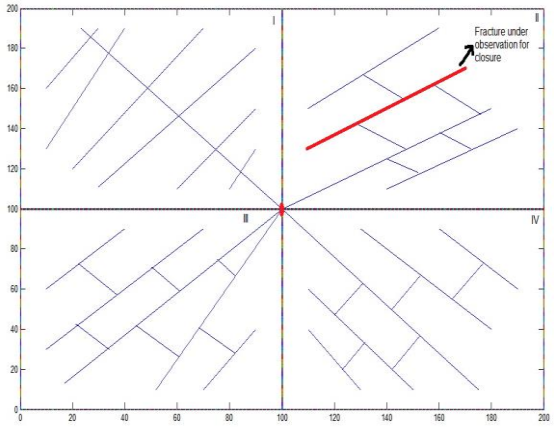

Fig. 4. Plan view of the rock fracture network (37 fractures) discretized into four blocks of I, II, III and IV. The producer well is located right in the middle.

In the first step the full permeability tensor of the reservoir is calculated by assuming a mean fracture aperture along each fracture; the resulting tensors are shown as permeability ellipses in Figure 5. The diameters of each ellipse show the principal permeability tensor entries. One can see from Figures Figures 4 and 5 that the orientation of each ellipse matches very well with the orientation of dominant fractures in the respective block.

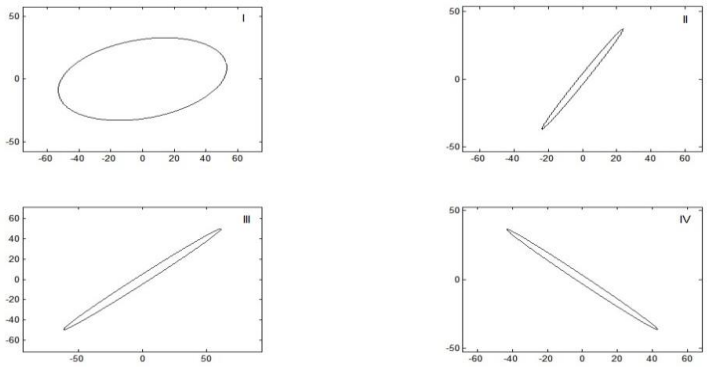

Fig. 5. The initial permeability ellipses for blocks I, II, III and IV, as shown in Fig. 4. Axes are permeabilities in mD.

4. Results and discussion

4.1. Production-induced change in the fracture aperture

As discussed above, NFRs can be stress sensitive to various extents. In other words, over the course of production, fracture opening reduces, resulting in significant reduction in permeability of the reservoir. We define the dimensionless cumulative reduction in the aperture as the cumulative reduction in fracture aperture at the current time step divided by the initial fracture aperture $\Delta b_i/b_{0,}$. The change in the dimensionless cumulative reduction in the aperture for a given fracture (Fig. 4) is shown in Figure 6 for two different boundary conditions of fluid flow, namely constant-flowing bottom-hole pressure (BHP) and constant flow rate at the wellbore. It can be seen from Figure 6 that as production progresses, fracture aperture reduces as a result of the decrease in the pore pressure and increase in the effective stress exerting orthogonally on the fracture wall.

One can see from Figure 6 that the change in the fracture aperture at the onset of production is dramatic. For instance, there is about 55% and 58% fracture closure for the two cases of constant flow rate and constant BHP, respectively. This is because of a sharp decrease in the pore pressure of the surrounding area to the wellbore at the early stage of production, which results in a rapid increase in effective stress acting on fractures, thereby leading to closure of fractures. This signifies the important role of fractures located adjacent to the wellbore in fluid flow. It is worth mentioning that even though these fractures are prone to marked closure at the production kick-off, their contribution in fluid flow towards the wellbore is obviously more significant than those fractures located further away from the wellbore.

Figure 6 also shows that the trend of change in dimensionless fracture aperture with respect to production time is linear for the case of constant flow rate after the early dramatic change. For the case of constant BHP, however, the fracture closes more rapidly over earlier times than later times.

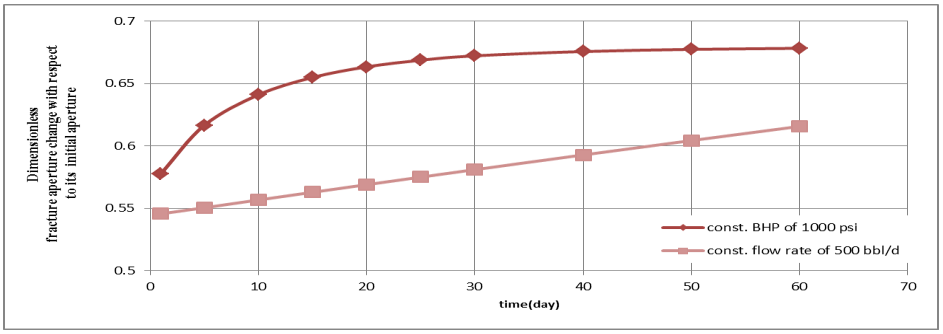

Fig. 6. Dimensionless change in aperture of the fracture marked in Figure 4 for two cases of constant bottom-hole pressure of 1000 psi and constant flow rate of 500 bbl/day.

4.2. Production-induced change in the shape of permeability ellipse

Initial permeability ellipses have been presented above in Figure 5. The effect of depletion on the shape of permeability ellipse of block I is shown in Figure 7. As shown, both ellipse diameters decrease with the progress of production. Again, one can see that the early decrease in the ellipse diameters (representing principal permeabilities) is dramatic.

4.3. Production-induced change in the entries of permeability tensor

Changes in permeability tensor entries of block I over production are shown in Figure 8. It can be seen that all permeability entries are affected by fracture closure resulting from pore-pressure reduction. For example, k_{xx} and k_{yy} decrease from 53 mD and 32 mD to 14 mD and 9 mD, respectively, during the first 25 days of production. The change percentages of the entries of the permeability tensor corresponding to block I are shown in Figure 9. This figure shows that the early change in all entries is far larger than the late change. It can also be seen that a reduction of up to 70% in all permeability tensor entries can take place over the first 20 days of production. The above results show the significance of the depletion effect on all permeability tensor entries. This effect is more pronounced at the early stage of production, and particularly for zones near the wellbore.

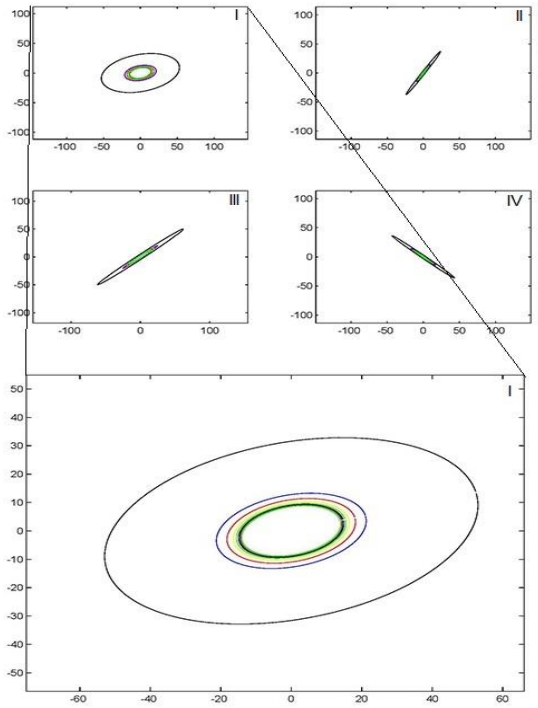

Fig. 7. Production-induced change in the shape of permeability ellipses over the course of production for four blocks of the NFR under consideration. Axes are permeabilities in mD. The largest ellipse corresponds to the initial permeability tensor prior to production. The next ellipses correspond to one, five, and 10 days of production, respectively.

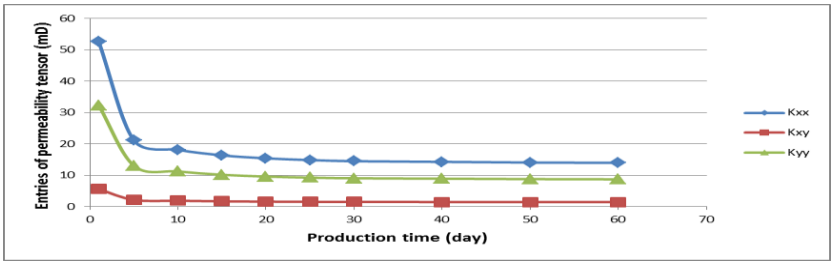

Fig. 8. Changes in permeability tensor entries vs. production time for block I. Results are obtained for the boundary condition of constant BHP of 1000 psi applied at the wellbore.

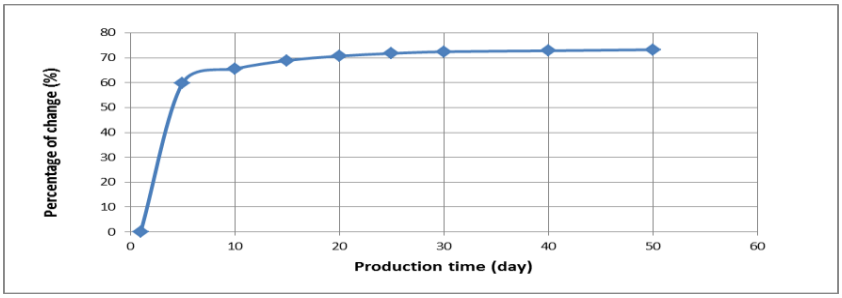

Fig. 9. Percentage of change in permeability tensor entries for the same block and boundary condition

4.4. Effect of production-induced fracture closure on production estimate

In order to show the importance of the depletion effect on the production estimate, two cases are considered. In the first case, the permeability tensor of each block is kept constant; in the second, the permeability tensor of each block changes as pore pressure decreases during production. The cumulative production for these two cases is shown in Figure 10. A lower cumulative production estimate is obtained for the dynamic permeability tensor. This echoes the fact that formation permeability decreases with production.

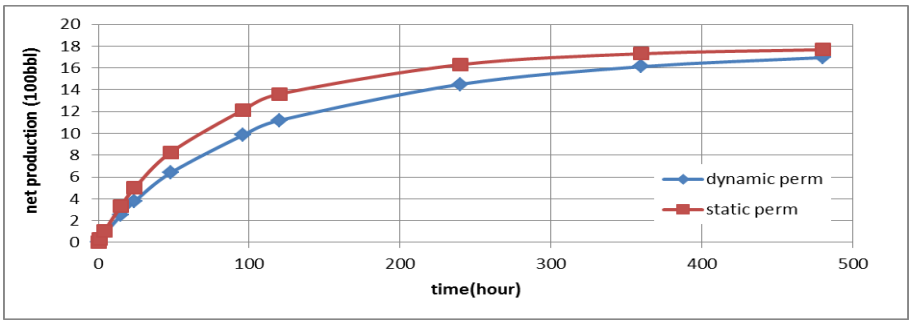

Fig. 10. Cumulative production vs. time

5. Parametric study

As explained above, the reduction in pore pressure during production causes fracture closure. This closure depends on the rock mechanical properties, i.e., Young's modulus and Poisson's ratio. If the production-induced fracture closure and its effect on the reservoir permeability is neglected, the volume of produced fluid and hence the production estimate will be determined inaccurately.

5.1. Effect of rock mechanical properties on percentage error in production estimate

Figures 11 and 12 show the effect of rock mechanical properties of the formation, i.e., Young's modulus and Poisson's ratio, on the relative error in production estimate caused by neglecting production-induced fracture closure.

As can be seen from Figure 11, the percentage of error in production estimate is lower for stiffer formations. For instance, the relative error in estimating production decreases from about 16% to approximately 4% (i.e., about one fourth) when the Young's modulus of the formation increases from about 4×10^6 psi to a magnitude of about 8×10^6 psi (i.e., about twice). These results show that the depletion effect on fracture closure and permeability, and thus in fluid production and forecasting, is more significant for formations with low modulus of elasticity. In other words, less-stiff reservoirs are less sensitive to the depletion effect on fluid flow.

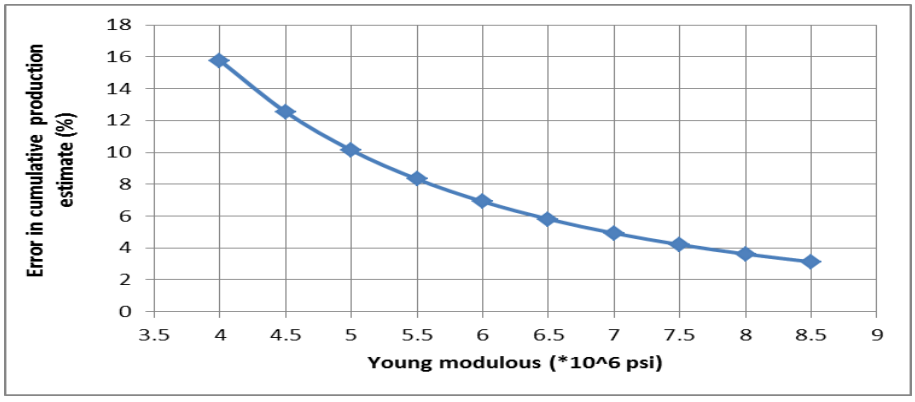

Fig. 11. Effect of Young's modulus on percentage error in cumulative production estimate after 20 days of production. Reservoir permeability is considered as a dynamic tensor.

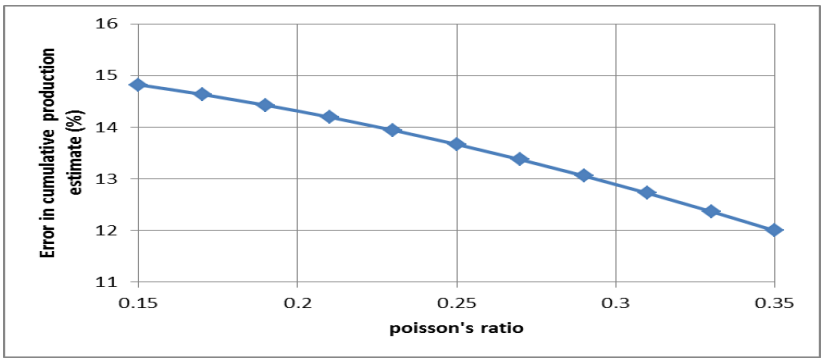

Fig. 12. Effect of Poisson's ratio on percentage error in cumulative production estimate after 20 days of production. Reservoir permeability is considered as a dynamic tensor.

Figure 12 shows that neglecting production-induced fracture closure on fluid flow results in greater percentage of error in production estimate for formations with lower Poisson's ratio. For example, the relative error in estimating production decreases from about 14.8% to approximately 12.9% when the Poisson's ratio of the formation increases from about 0.15 to about 0.3.

5.2. Effect of initial fracture aperture

The effect of initial aperture on relative percentage error in production estimation for various production periods is shown in Figure 13. It can be seen that for earlier production times the effect of depletion on fracture closure is more significant where the initial fracture aperture is greater. For example, after five days of production, the percentage of error in production estimate caused by overlooking depletion-induced fracture closure decreases from nearly 50% to almost 30% where the initial fracture aperture is assumed to be 30% less (equal to $0.7b_0$). This effect however, loses its significance for long production periods.

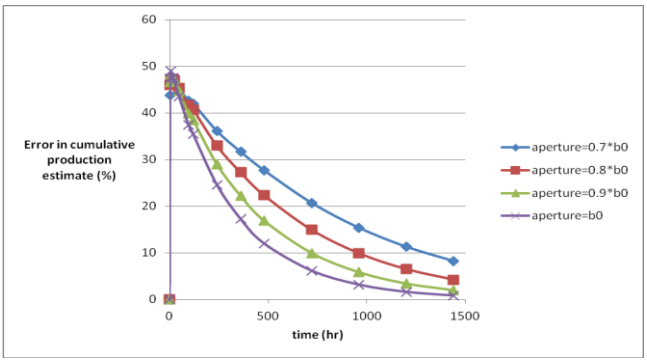

Fig. 13. Effect of initial aperture on percentage error involved in production estimate as a function of production time

6. Conclusion

An integrated approach for modelling fluid flow in fractured reservoirs has been presented. This paper has shown that this approach can be efficiently used for evaluation of full permeability tensor as well as production-induced change in permeability tensor of naturally fractured reservoirs. This model clearly shows that fracture aperture is reduced during production. The results also show that the fractures close more rapidly in the early period of production (up to 55% of the initial value). Furthermore, we have seen that permeability ellipses become significantly smaller as a result of reservoir depletion-induced reduction in permeability tensor entries, both diagonals and off-diagonals. An up-to-70% decrease in reservoir permeability can result from depletion. We have also shown that where reservoir rock mechanics properties, i.e., Young's modulus and Poisson's ratio, are lower, the permeability of the reservoir is more sensitive to the depletion effect. If the depletion-induced reduction in

permeability tensor is neglected, a considerable percentage error in production estimate is involved. For the case considered in this paper, an up-to-12% difference between the productions of the two cases, i.e., with and without accounting for depletion effect on permeability tensor, was observed over the first 20 days of production.

Nomenclature

A: measured area of the plan-view rock face, ft^2.
B: formation volume factor, bbl/STB.
b_k: aperture of the k^{th} fracture, ft.
b_0: initial average aperture, ft.
Δb_i: change in fracture aperture at the current time step, ft.
c: pore volume compressibility, psi^{-1}.
c_t: total system compressibility, psi^{-1}.
Ei: exponential integral function.
E: Young's modulus, psi.
f: force vector.
h: pay-zone thickness, ft.
H: mass matrix.
k: permeability tensor, mD.
k_{ij}: equivalent permeability tensor, mD.
k_{xx}, k_{xy}, k_{yy}: components of the permeability tensor, mD.
L_k: length of the k^{th} fracture, ft.
L: fracture length, ft.
L: mass matrix.
M: mass matrix.
N: number of fractures.
n_i and n_j: unit normal vectors.
ne: number of elements.
N_1, N_2 and N_n: shape functions of the first, second and n^{th} elements.
P_{ij}: second-rank tensor describing the geometry of joints, ft^2.
P: pressure vector, psi.
p_1, p_2 and p_n: pore pressure of first, second and n^{th} node, respectively, psi.
p_i: initial reservoir pressure, psi.
$\bar{p}$: average pressure of the element, psi.
q: the flow rate, STB/day.
t: time, s, day.
V_p: volume of the reservoir block at pressure p, ft^3.
V_i: initial volume of the reservoir block, ft^3.
x, y: coordinates in 2-D Cartesian system.
δ_{ij}: Kronecker delta, dimensionless.
λ: geometric factor, dimensionless.
$\emptyset_t$: total effective porosity, dimensionless.
μ: fluid viscosity, cp.
δ: change in fracture aperture or fracture closure.
ν: Poisson's ratio, dimensionless.
σ'_n: normal effective stress, psi.
ζ: ratio reflecting surface topography, dimensionless.

SI Metric Conversion Factors

bbl x 1.589873 E-01=m^3

cp x 1.0 E+00=Pa.s

ft x 3.048 E-01=m

ft^3 x 9.290304 E-02=m^3

psi x 6.894757 E+00=kPa

mD x 9.869233 E-16=m^2

References

[1] Kunkel, J.R., Way, S. C., and McKee, C. R. (1988). Comparative Evaluation of Selected Continuum and Discrete-fracture Models: Creston Study Area, Eastern Washington. US Nuclear Regulatory Commission.

[2] Schwartz, F.W. and Smith, L. (1988). A continuum approach for modelling mass transport in fractured media. Water Resources Research, 24(8): pp. 1360-1372.

[3] Long, J.C.S., Remer, S., Wilson, C.R. and Witherspoon, P.A. (1982). Porous media equivalents for network of discontinuous fractures. Water Resources Research, 18(3): pp. 645-658.

[4] Therrien, R. and Sudicky, E. (1996). Three-dimensional analysis of variably-saturated flow and solute transport in discretely-fractured porous media. Journal of Contaminant Hydrology, 23(1): pp. 1-44.

[5] Barenblatt, G.I., Zheltov, Y.P. and Kochina, I.N. (1960). Basic concepts on the theory of seepage of homogeneous liquids in fissured rocks. Prikladnaya Matematika i Mekhanika,. 24(5): pp. 852-864.

[6] Chilingarian, G.V., Mazzullo, S.J. and Rieke, H.H. (1992). Carbonate reservoir Characterization: A Geologic -Engineering Analysis. Developments in Petroleum Science,

ed. G.V. Chilingarian, S.J. Mazzullo, and H.H. Rieke. Vol. 30, Part I., Amsterdam: Elsevier Publ. Co.

[7] Chilingarian, G.V., Mazzullo, S.J. and Rieke, H.H. (1996). Carbonate reservoir Characterization: A Geologic -Engineering Analysis. Developments in Petroleum Science, 44, ed. G.V. Chilingarian, Vol. 44, Part II., Amsterdam: Elsevier Publ. Co.

[8] Bagheri, M.A. and Settari, A.T. (2006). Modelling fluid flow in deformable fractured reservoirs using full tensor permeability, Golden Rocks 2006, The 41st US Symposium on Rock Mechanics (USRMS), American Rock Mechanics Association.

[9] Hughes, R.G. and Blunt, M.J. (2001). Network modelling of multiphase flow in fractures. Advances in Water Resources, 24(3): pp. 409-421.

[10] Long, J.C.S. and Witherspoon, P.A. (1985). The relationship of the degree of interconnection to permeability in fracture networks, Journal of geophysical research, 90(B4): pp. 3087- 3089.

[11] Oda, M. (1985). Permeability tensor for discontinuous rock masses. Geotechnique,. 35(4).

[12] Renard, P. and De Marsily, G. (1997). Calculating equivalent permeability: a review. Advances in Water Resources, 20(5): pp. 253-278.

[13] Lough, M., Lee, S. and Kamath, J. (1998). An efficient boundary integral formulation for flow through fractured porous media. Journal of Computational Physics, 143(2): pp. 462-483.

[14] Snow, D.T. (1968). Rock fracture spacings, openings, and porosities, Journal of Soil Mechanics & Foundations Div.

[15] Snow, D.T. (1969). Anisotropie permeability of fractured media, Water Resources Research,. 5(6): pp. 1273-1289.

[16] Matheron, G., et al. (1987). Conditional simulation of the geometry of fluvio-deltaic reservoirs. in SPE Annual Technical Conference and Exhibition, Society of Petroleum Engineers.

[17] Dagan, G., (1993). Higher-order correction of effective permeability of heterogeneous isotropic formations of lognormal conductivity distribution. Transport in Porous Media, 12(3): pp. 279-290.

[18] elhar, L.W. (1993). Stochastic subsurface hydrology, Prentice Hall PTR.

[19] Cacas, M., et al., (1990). Modelling fracture flow with a stochastic discrete fracture network: Calibration and validation: 1. The flow model, Water Resources Research, 26(3): pp. 479-489.

[20] Durlofsky, L.J. (1991). Numerical calculation of equivalent grid block permeability tensors for heterogeneous porous media, Water resources research, 27(5): pp. 699-708.

[21] Nakashima, T., Arihara, N. and Sato, K. (2001). Effective permeability estimation for modelling naturally fractured reservoirs. SPE Middle East Oil Show.

[22] Jones, F.O., Jr., (1975). A Laboratory Study of the Effects of Confining Pressure on Fracture Flow and Storage Capacity in Carbonate Rocks.

[23] Buchsteiner, H., Warpinski, N.R. and Economides, M.J. (1993). Stress-Induced Permeability Reduction in Fissured Reservoirs, SPE Paper 26513.

[24] Lorenz, J.C. (1999). Stress-Sensitive Reservoirs. JPT, pp. 61-63.

[25] Abass, H., et al. (2007). Understanding Stress Dependant Permeability of Matrix Natural Fractures and Hydraulic Fractures in Carbonate Formations. in SPE Saudi Arabia Section Technical Symposium, Society of Petroleum Engineers.

[26] Nelson, R. (2001). Geologic Analysis of Naturally Fractured Reservoirs, Elsevier Science.

[27] van Golf-Racht, T.D. (1982). Fundamentals of Fractured Reservoir Engineering, Elsevier Science.

[28] Duan, Y., et al. (2000). Closure Behaviour of Natural Rock Fractures, SPE/AAPG Western Regional Meeting.

[29] Economides, M.J., Hill, A.D. and Ehligh_Economides, C.A. (1993). Petroleum Production Systems., New Jersey, Prentice Hall.

[30] Papadopulos, I.S. (1965). Nonsteady flow to a well in an infinite anisotropic aquifer, in Proceedings of the Dubrovnik Symposium on the Hydrology of Fractured Rocks, International Association of Scientific Hydrology.